Sharp interface in epitaxial graphene layers on 3*C*-SiC(100)/Si(100) wafers

A. Ouerghi,[1] M. Ridene,[1,*] A. Balan,[2] R. Belkhou,[3] A. Barbier,[4] N. Gogneau,[1] M. Portail,[5] A. Michon,[5] S. Latil,[4] P. Jegou,[4] and A. Shukla[2]

[1]*Laboratoire de Photonique et de Nanostructures (CNRS-LPN), Route de Nozay, F-91460 Marcoussis, France*

[2]*Université Pierre et Marie Curie (CNRS-IMPMC), Rue de Lourmel, F-75015 Paris, France*

[3]*Synchrotron-SOLEIL, Saint-Aubin, BP48, F-91192 Gif sur Yvette, France*

[4]*CEA-Saclay, DSM/IRAMIS/SPCSI, F-91191 Gif sur Yvette, France*

[5]*CNRS-CRHEA, Rue Bernard Grégory, F-06560 Valbonne, France*

(Received 29 November 2010; revised manuscript received 25 February 2011; published 25 May 2011)

Graphene ranks highly as a promising material for future nanoelectronic devices because of its exceptional electron-transport properties. It appears as a material of choice for high-frequency applications. We report the growth and structure of epitaxial graphene layers on 3*C*-SiC(100)/Si(100) wafers using low-energy electron microscopy. Selective-area low-energy electron diffraction highlights the presence of two graphene domains, rotated by $\pm 15^{\circ}$ with respect to the SiC lattice. Micro-Raman spectroscopy demonstrates the characteristic signature of few layer graphene on the SiC. X-ray photoemission spectroscopy evidences a sharp interface between graphene and 3*C*-SiC(100). It appears that epitaxial graphene layers obtained on 3*C*-SiC(100)/Si(100) have properties similar to those obtained using classical 6*H* or 4*H*-SiC substrates with the advantage of being compatible with the current Si processing technology.

DOI: 10.1103/PhysRevB.83.205429 PACS number(s): 68.65.Pq, 61.48.Gh, 61.05.jh

I. INTRODUCTION

Graphene is a promising material that is expected to have the potential to revolutionize materials physics as well as much of present day electronics technologies. While its properties make it an ideal material for the next generation of electronics, concerns about the technological feasibility of industrial scale graphene devices recently emerged. It is important to recognize that the extraordinary fundamental properties of a novel material do not necessarily translate easily into technological innovations and eventual implementation into applications.[1,2]

Graphene is at the center of a significant research effort. Near-ballistic transport at room temperature and high mobility make it a potential material for nanoelectronics, especially for high-frequency applications.[3,4] These peculiar properties have led many investigators to expect that graphene could be used to overcome the Si devices limitations especially when considering high charge mobility. Different elaboration methods have been prospected in recent years to produce graphene layers. Conventional techniques, such as the micromechanical exfoliation of isolated graphene from bulk graphite has been developed[2,5] or, alternatively, the graphitization of bulk SiC under argon atmosphere produce few layers graphene (FLG) with a considerably larger domain size than that previously attainable.[6]

In the perspective of industrial-scale fabrication and mass production, the two last techniques are not of practical interest because these methods give access only to limited small wafers and SiC substrate technology is still expensive compared to standard Si-based 4-in. technology. Developing graphene synthesis methods able to overcome these limitations is very challenging and is a mandatory step prior to the industrial use of graphene layers. The synthesis of epitaxial graphene on SiC epitaxial layers on silicon wafers is an attractive method, which presents several advantages: (i) the ability to produce substrates significantly larger than commercial bulk SiC substrates wafers; (ii) compatibility with current Si processing techniques, which should make the graphene technology attractive from an industrial viewpoint; (iii) epitaxial graphene presents similar properties to those of graphene on 6*H*-SiC(0001).

Recently, we have shown that it is possible to grow epitaxial graphene on 3*C*-SiC/Si(111) by depletion of Si from the SiC surface. In particular, we show that graphene exhibits remarkable continuity of step edges suggesting the possibility of growing large scale graphene layer with linear dispersion at the *K* point of the Brillouin zone.[7,8] Epitaxial graphene on 3*C*-SiC(100) has been studied using near-edge x-ray-absorption fine-structure spectroscopy and angle-resolved photoemission spectroscopy (ARPES) by Aristov *et al.*[9] In the present work, we provide direct observation of an epitaxial graphene structure on 3*C*-SiC(100) epitaxial layer on silicon wafer using μ-beam low-energy electron diffraction (μ-LEED) and low-energy electron microscopy (LEEM). The interface sharpness between FLG and the 3*C*-Si(100) is demonstrated through the investigation of the electronic structure of epitaxial graphene by means of photoemission spectroscopy (XPS) and micro-Raman spectroscopy.

II. EXPERIMENTAL DETAILS

The 3*C*-SiC epilayers (1500 nm) used in this work were grown on Si(100) wafer in chemical vapor deposition (CVD) reactor. The deposition is made within a resistively heated hot wall reactor using silane and propane gases as precursors diluted in hydrogen. The surface of these heteroepitaxial materials is typically characterized by antiphase domain (APD) boundaries. *3C*-SiC/Si(100) pseudosubstrate were first outgassed for several hours at 600 °C under UHV conditions and then annealed under a Si flux (2 Å/min) at 700 °C to remove the native oxide. Our graphene layers were elaborated following the approach described previously for the 3*C*-SiC(111) pseudosubstrate.[7] The graphitization is achieved between 1150 and 1300 °C, the growth is monitored using LEED. The samples were further cooled down to room temperature and transferred *ex situ* in air for characterization. Once introduced in the LEEM or XPS analysis chambers,[10] the samples were

outgassed for 1 h at 600 °C prior to measurements in order to desorb any air-exposure residual contaminant. In the LEEM instrument (Elmitec GmBH–LEEM III), the electron gun and sample were biased at 20 kV. The bias difference between the electron gun and sample is the start voltage V_{ST} and eV_{ST} is roughly equal to the primary electron-beam energy. The bright-field (BF) and dark-field (DF) LEEM images have been obtained by selecting the corresponding LEED spots via an aperture (contrast aperture) placed on the optical path of the microscope column. XPS experiments were carried out on a Kratos analytical system using an Al K_α monochromatized (1486.6 eV) source with an overall energy resolution of ~350 meV. The spectra were deconvoluted using a Doniach-Sunjic approach after linear or Shirley-type background subtraction. Micro-Raman spectroscopy was performed at room temperature with a Renishaw spectrometer using a 514-nm argon laser focused on the sample by a DMLM Leica microscope with a 50x (NA = 0.75) objective. The Rayleigh diffusion was eliminated by edge filters. Presence of the two-dimensional (2D) band at 2700 cm^{-1} was used to monitor epitaxial graphene. Finally, the surface morphology was studied by atomic-force microscopy (AFM), in tapping mode.

III. RESULTS AND DISCUSSION

LEED patterns have been used to monitor surface structural changes and graphene formation. The Si-rich (3×2) and (2×1) surfaces are obtained by *in situ* annealing without Si flux. The transition from the Si- to the C-rich surface due to the sublimation of Si surface atoms takes place in the 1050 to 1100 °C temperature range. Under the effect of annealing between 1100 and 1150 °C, the $c(2 \times 2)$ reconstruction begins to develop, this phase is usually interpreted as a *C*-terminated structure.[11] Further annealing induces the coexistence of the graphene layers and the (2×1) reconstruction of 3*C*-SiC(100). Annealing above 1200 °C is required to develop the (1×1) graphitic phase on the SiC pseudosubstrate. Figure 1(a) shows typical diffraction patterns of graphene layers for a sample annealed at 1200 °C for 10 min. The LEED experiment has been performed on a LEEM microscope setup. The μ-LEED pattern is collected over a small area of the sample (10 μm^2) allowing us to investigate the structural homogeneity of the sample surface. Two contributions can be clearly distinguished in the μ-LEED pattern. The first contribution is characteristic of the 3*C*-SiC(100) lattice (square indicated by black boxes). The second feature is represented by two hexagonal lattices (shown by blue and red arrows) confirming the presence of graphene layers on top of the 3*C*-SiC(100). This behavior can be understood as the result of any of the following two phenomena:

(i) Our heteroepitaxial 3*C*-SiC/Si(100) typically include antiphase domain (APD) with respect to the Si(100); that is, two domains rotated by 90° with respect to each other. A graphene domain oriented with +15° to the [110] direction of the inphase/antiphase 3*C*-SiC(100) domains will appear at ±15° in the LEED images [Fig. 1(b)].

(ii) A possible alternative consists of the presence of two hexagonal lattices rotated by ±15° with respect to a single domain square SiC lattice [Fig. 1(d)].

On the same sample but at a different location on the surface we observed some inhomogeneites in the orientations of the

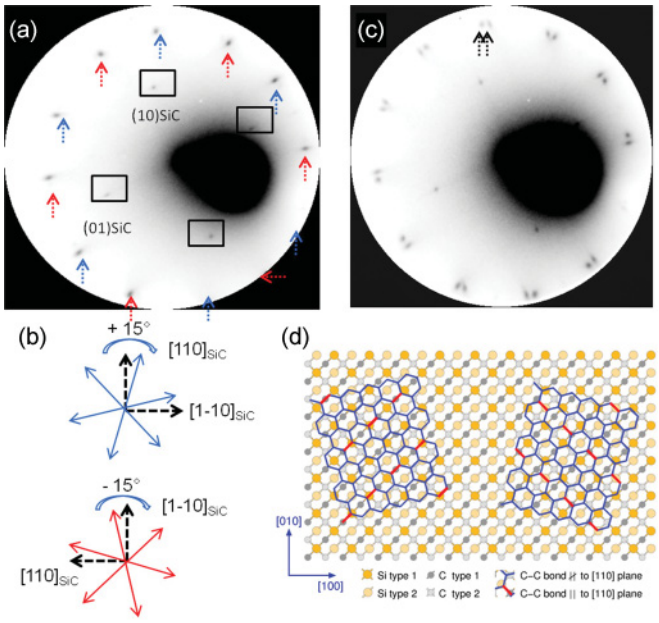

FIG. 1. (Color online) (a) μ-LEED image ($Ep = 46$ eV) of epitaxial graphene (1.5 layer) on 3*C*-SiC(100). The intense bright large spot is due to backscattered secondary electrons. (b) Crystallographic axes of the cubic substrates and graphene layer as determined from the LEED. (c) μ-LEED image ($Ep = 46$ eV) of another area of epitaxial graphene on 3*C*-SiC(100) characterized by four hexagonal graphene on 3*C*-SiC(100). (d) Epitaxial of sixfold versus fourfold lattices [graphene versus 3*C*-SiC(100)]; Si (type 1) and C (type 1) correspond to the first layer and Si (type 2) and C (type 2) corresponds to the second layer of 3*C*-SiC(100) substrate.

graphene planes with respect to the SiC lattice. Other than the ±15° explained before we observe an additional ±2° misalignment [Fig. 1(c)]. This rotation can happen between two domains in the same first graphene layer or between the first layer and the second layer. From the μ-LEED image, we may thus conclude that our graphene pattern consists mainly of two hexagonal lattices rotated by ±15° (±2°) with respect to the square 3*C*-SiC lattice. This would be in agreement with the superstructures observed in the case of graphene grown on C terminated 6*H*-SiC for which a moiré pattern is obtained, due to a misorientation between the two topmost carbon layers.[12]

The graphene sample was further characterized by LEEM microscopy in order to evaluate the thickness spatial distribution.[13,14] Figure 2 shows bright-field (BF) and dark-field (DF) LEEM images from the regions observed by μ-LEED [Fig. 1(a)]. Figures 2(a) and 2(b) shows a typical BF LEEM pattern from graphene layer.

The electron energies *Ei*, are (a) 2.69 and (b) 3.52 eV. These images show that the image intensity levels in different regions change with the energy in different manners. The layer exhibits large regions separated by thin black lines. Hence we do not currently exclude the presence of fine structures caused by the thickness distribution (monolayer or bilayer) in antiphase domain. This behavior can be understood as the result of our graphene layer has probably two hexagonal lattices rotated by ±15° with respect to the square SiC lattice.

DF images from the two SiC LEED spots "$(01)_{SiC}$" and "$(10)_{SiC}$" in Fig. 1 are shown in Figs. 2(c) and 2(d). These

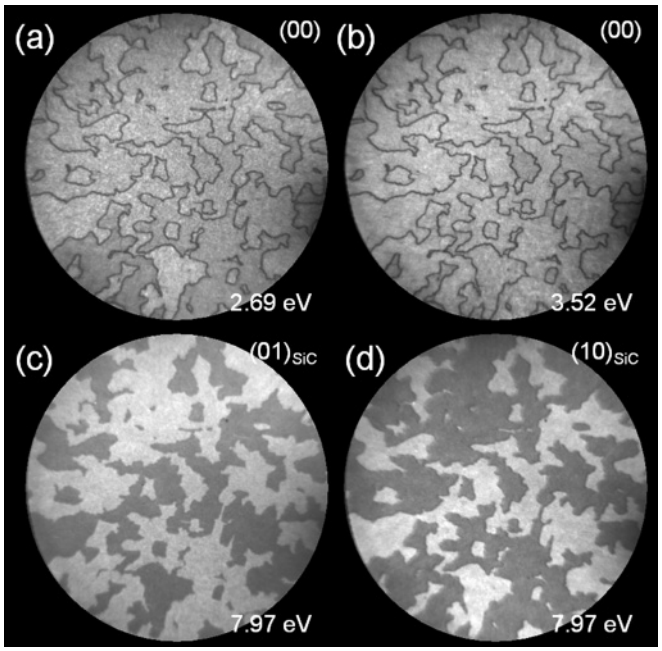

FIG. 2. LEEM images, taken from the FLG sample annealed at 1200 °C (1.5 layer) (a) bright-field image ($V_{ST} = 2.69$ eV); (b) bright-field image ($V_{ST} = 3.52$ eV); (c) Dark-field image ($V_{ST} = 7.97$ eV) for the $(01)_{SiC}$ LEED spot; (d) Dark-field image ($V_{ST} = 7.97$ eV) for the $(10)_{SiC}$ LEED spot. The microscope field of View is 25 μm.

two DF images clearly show that for some regions of the sample the intensity is reversed depending on which LEED spot has been considered. This indicates that the domains of 3*C*-SiC(100) have twofold symmetry. Due to the alternating layer stacking sequence in the [001] crystallographic direction of 3*C*-SiC(100), the substrate surface possesses only a twofold symmetry, which would necessarily imply that only one of the domains should be present. The presence of both domains indicates that the 3*C*-SiC surface presents two distinct epitaxial orientations with respect to the Si(100) pseudosubstrate: [100]//[100] or [100]//[010].[15]

The direct comparison of the BF image with the two DF images clearly indicates that the black lines between the terraces of graphene layers (BF image) can be correlated with the boundaries of the twofold symmetry of the 3*C*-SiC(100). We thus establish that the graphene terraces are bordered by the domains of the pseudosubstrate.

An important question that we can ask concerns the factors that limit the size of graphene domains. Within a given APD the free SiC(100)/Si(100) surface before graphitization shows a morphology with steps or terraces.[15] The question arises whether these can also limit graphene domain size, like APD boundaries. Figure 3(a) shows an AFM image of the graphene layer studied by LEEM after surface graphitization at 1200 °C. Within a given APD, the AFM images reveal atomically flat terraces with no step or edges. Graphene forms a smooth layer thanks to a carpetlike behavior which drapes the edges without interruption [Fig. 3(b)]. The graphene domains are not limited by the width of the SiC terraces but rather by its surface symmetry and the APDs as deduced from the LEEM and AFM images. This finding indicates the possibility to

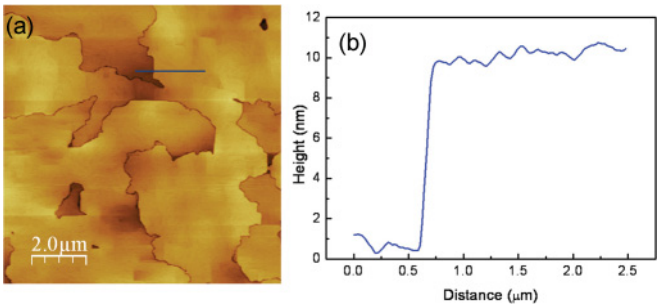

FIG. 3. (Color online) (a) AFM image of epitaxial graphene annealed at 1200 °C (1.5 layer); (b) line section profile displaying the surface height of the SiC(100) after epitaxial graphene formation. The steps height corresponds to ADPs boundaries of 3C-SiC(100).[13]

control and grow large scale graphene on 3*C*-SiC(100) beyond the SiC terraces. Interestingly, the continuity of the graphene layer observed here is in agreement with the results obtained for the growth of graphene layers on 6*H*-SiC(0001) vicinal substrates, where a carpetlike growth mode covering several substrate terraces and steps was observed by atomically resolved STM and AFM images.[16,17]

We measured Raman spectra on the same sample at room temperature with a micro-Raman spectrometer. The measurements were performed for the $c(2 \times 2)$-3*C*-SiC(100) reconstructed and two different stages (1.5 and 2.8 layers) of the epitaxial graphene layer. The key Raman results of graphene on 3*C*-SiC(100) are displayed in Fig. 4. The $c(2 \times 2)$ reconstruction of SiC(001) has several overtone peaks in the 1000–2000 cm^{-1} regime. The peak at 1516 cm^{-1} is considered to be an overtone of the *L*-point optical phonon. The Raman signals from the two graphene layers show prominent characteristic graphene peaks at 1600 cm^{-1} (*G*) and 2732 cm^{-1} (2D), which give evidence of carbon sp^2 reorganization. The *G* peak value of 1600 cm^{-1} could indicate strong *n* doping. Also the blueshifted position of the 2D peak at 2732 cm^{-1} indicates compressive strain of the graphene layer during the post-growth cooling down procedure or charge-transfer doping from the substrate. The blueshift of the *G* and 2D band has also been reported in epitaxial graphene on 6*H*-SiC wafers.[18–20]

The Lorentzian shape of the 2D feature is a feature of epitaxial graphene layers and the signature of a system with a single-band electronic dispersion. The 2D peak is, however,

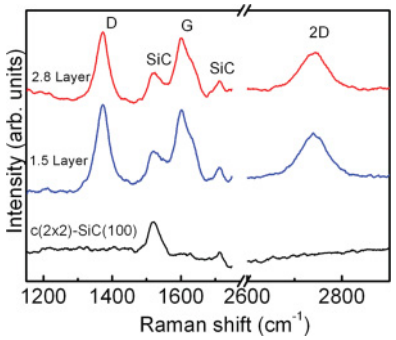

FIG. 4. (Color online) Micro-Raman characterization of graphene/3*C*-SiC(100): Comparison of Raman spectra taken on the c-(2×2) surface reconstruction and on two graphene layers.

much broader with a full width at half maximum (FWHM) of around 80 cm^{-1}. The broadening can be attributed both to defect scattering and two or more layer graphene following Ni *et al.*[18] The strong intensity of the *D* peak (in comparison to the *G* peak) is a clear indication of zone-boundary phonons scattering on defects, not allowed in ideal graphene due to the large wave vector of the *K*-point phonon involved. Its presence is an indication of disorder, such as finite-size domains, in agreement with previous measurements on the epitaxial graphene on 4*H*-SiC(000-1).[18] The defects including vacancies and lattice distortions are attributed to the two domains of graphene on SiC(100) and/or APDs boundaries (Fig. 1), as well as to twisting, corrugation, and steps edges. The ratio of the intensities of the *G* peak and *D* peak gives an average distance between defects on the order of 10 nm.[18]

We next used XPS to demonstrate the absence of an interface layer between the first graphene layer and the SiC(100) pseudosubstrate. This is supported by the C 1*s* core-level peak analysis and deconvolution for the 3*C*-SiC(100) surface and for the two stages of FLG growth, as shown in Fig. 5. The C 1*s* for the $c(2 \times 2)$-SiC(100) surface has two components: one is related to the bulk component (*B*) in SiC and the other one to the surface component (*S*), shifted by 1.2 eV toward higher binding energy. The peak position together with the *S*/*B* intensities branching ratio are a specific signature of the $c(2 \times 2)$-SiC(100) surface reconstruction. The surface structure corresponds to the C-C dimers in a *sp* configuration having a triple bond located on the topmost atomic layer.[10,11] For the FLG, the SiC bulk component appears at 282.9 eV at binding energy and the graphene-related component (*G*) is shifted by 1.4 eV toward higher binding energy with respect to the bulk SiC position. The surface peak of the $c(2 \times 2)$ reconstruction disappeared due to the formation of graphene on 3*C*-SiC. The *G* peak indicates sp^2 hybridized C-C bonds, which is a signature of the graphene layers. After graphitization starts there is no signal corresponding to the interface between the graphene layers and the substrate [Fig. 5(a)]. Finally, in order to confirm the absence of additional components, the *C*1*s* spectra of the graphene and 3*C*-SiC(100) were recorded using varying probing depth [Fig. 5(b)], i.e., varying the analyzer angle in order to identify surface or bulk-related components. It is very interesting to point out that the substrate peak SiC changes significantly in intensity with probing depth, but we do not observe any change in the line shape or the peak position of the graphene peak *G*. This indicates that the *G* peak has a single component. More precisely, this finding confirms the absence of an interfacial graphitic layer covalently bound to the 3*C*-SiC(100). In agreement to epitaxial graphene on SiC(000-1), only two components can be resolved on FLG (Fig. 5).[21,22]

Our results clearly indicate that the FLG/3*C*-SiC(100) interfaces are abrupt. XPS and Raman spectroscopy exhibit, respectively, a feature component at 284.6 eV and 2D band for the first epitaxial carbon layer (Figs. 4 and 5). From these observations we conclude that the first graphitic layer grows on top of the 3*C*-SiC(100) without interface structure, which therefore can be considered to be a graphene layer with a single-layer (Dirac-like) band structure. It must be underlined that the growth of the first graphene layer on 3*C*-SiC(100) is similar to that reported for the 6*H*-SiC(000-1) substrates[21,23,24]

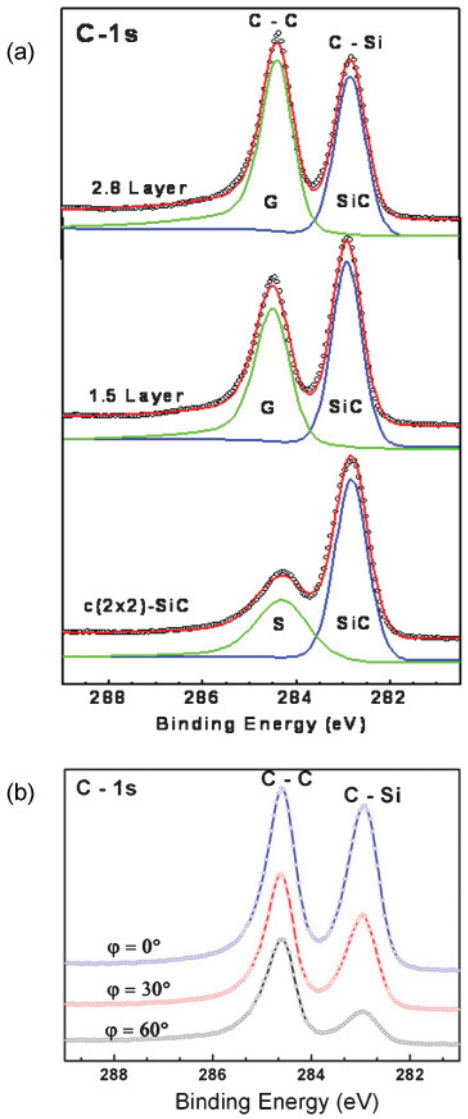

FIG. 5. (Color online) (a) C-1*s* core level for graphene with a Doniach-Sunjic line-shape analysis of the two layers graphene grown on 3*C*-SiC(100) and $c(2 \times 2)$ surface reconstruction; the different components are labeled with respect to the carbon bonding. (b) C-1*s* XPS spectra of graphene on 3*C*-SiC(100) surface at different angle grazing incidence.

with, however, some specificities. In our case LEED images of graphene do not present a rotational disorder in contrast to previous observations of FLG on 6*H*-SiC(000-1) substrate, which exhibits a high degree of disorder. This shows that the interaction between graphene and the 6*H*-SiC(000-1) is much weaker than in the case of graphene on 3*C*-SiC(100).[25] This is the major difference with respect to graphene on 6*H*-SiC(0001) and graphene on 3*C*-SiC(111),[6,16,26,27] where the first graphene layer, while easy to grow uniformly, is nonconductive. Thus from an electronic and charge-carrier viewpoint, this layer is not graphene at all, but rather an "interface layer" on which additional, electrically active graphene must be grown. Band-structure measurements by means of ARPES and first-principles calculations show disruption of the interface layer π bands by strong covalent bonding to the SiC substrate

at the interface.[21,28] As a consequence of this strong interaction on the Si terminated face, π states are removed from the vicinity of the Fermi level for the interface layer and STM images do not reveal the graphenelike atomic lattice.[29]

IV. CONCLUSION

In summary, we have successfully grown graphene on 3*C*-SiC(100) epitaxial layers on silicon. The morphology of the graphene layers consisting of large and flat domains were confirmed by LEEM and AFM. The lateral domain size is only limited by the antiphase grain boundaries pre-existing in the 3*C*-SiC(100) substrate and not by steps or terraces within a domain. Raman spectroscopy and μ-LEED showed the presence of epitaxial graphene on 3*C*-SiC(100) with a two-domain hexagonal arrangement of carbon atoms. X-ray photoemission spectroscopy data demonstrate a sharp interface between the graphene layer and the substrate. In the initial stage of the growth, carbon atoms thermally released from the SiC substrate nucleate into a sp^2-hybridized layer and form a flat conductive graphene layer. This work brings different insights into the basic knowledge of the growth process of graphene layers on 3*C*-SiC(100)/Si(100). These encouraging results are fundamental steps toward the development of Si-based technologies for the production of graphene and will likely open new perspectives for industrial-scale fabrication.

ACKNOWLEDGMENTS

We are grateful to D. Martinotti for his outstanding efforts and the technical assistance during the LEEM experiments at the CEA/IRAMIS/SPCSI laboratory. A.O. thanks B. Etienne and L. Travers for fruitful discussion.

*Also at LPMC, Département de Physique, Faculté des Sciences de Tunis, Campus Universitaire, 1060 Tunis, Tunisia.

[1] K. S. Novoselov, A. K. Geim, S. V. Morozov, D. Jiang, M. I. Katsnelson, I. V. Grigorieva, S. V. Dubonos, and A. A. Firsov, Nature (London) **438**, 197 (2005).

[2] K. S. Novoselov, Z. Jiang, Y. Zhang, S. V. Morozov, H. L. Stormer, U. Zeitler, J. C. Maan, G. S. Boebinger, P. Kim, and A. K. Geim, Science **315**, 1379 (2007).

[3] A. Reina, X. Jia, J. Ho, D. Nezich, H. Son, V. Bulovic, M. S. Dresselhaus, and J. Kong, Nano Lett. **9**, 30 (2009).

[4] M. Orlita, C. Faugeras, P. Plochocka, P. Neugebauer, G. Martinez, D. K. Maude, A.-L. Barra, M. Sprinkle, C. Berger, W. A. de Heer, and M. Potemski, Phys. Rev. Lett. **101**, 267601 (2008).

[5] A. Shukla, R. Kumar, J. Mazher, and A. Balan, Solid State Commun. **149**, 718 (2009); A. Balan, R. Kumar, M. Boukhicha, O. Beyssac, J.-C. Bouillard, D. Taverna, W. Sacks, M. Marangolo, E. Lacaze, R. Gohler, W. Escoffier, J.-M. Poumirol, and A. Shukla, J. Phys. D **43**, 374013 (2010).

[6] K. V. Emtsev, A. Bostwick, K. Horn, J. Jobst, G. L. Kellogg, L. Ley, J. L. McChesney, T. Ohta, S. A. Reshanov, J. Röhrl, E. Rotenberg, A. K. Schmid, D. Waldmann, H. B. Weber, and T. Seyller, Nat. Mater. **8**, 203 (2009).

[7] A. Ouerghi, A. Kahouli, D. Lucot, M. Portail, L. Travers, J. Gierak, J. Penuelas, P. Jegou, A. Shukla, T. Chassagne, and M. Zielinski, Appl. Phys. Lett. **96**, 191910 (2010).

[8] A. Ouerghi, R. Belkhou, M. Marangolo, M. G. Silly, S. El Moussaoui, M. Eddrief, L. Largeau, M. Portail, and F. Sirotti, Appl. Phys. Lett. **97**, 161905 (2010).

[9] V. Y. Aristov, G. Urbanik, K. Kummer, D. V. Vyalikh, O. V. Molodtsova, A. B. Preobrajenski, A. A. Zakharov, C. Hess, T. Hänke, B. Büchner, I. Vobornik, J. Fujii, G. Panaccione, Y. A. Ossipyan, and M. Knupfer, Nano Lett. **10**, 992 (2010).

[10] A. Ouerghi, M. Marangolo, M. Eddrief, B. B. Lipinski, V. H. Etgens, M. Lazzeri, H. Cruguel, F. Sirotti, A. Coati, and Y. Garreau, Phys. Rev. B **74**, 155412 (2006); A. Ouerghi, J. Penuelas, C. Andreazza-Vignolle, P. Andreazza, N. Bouet, and H. Estrade-Szwarckopf, J. Appl. Phys. **100**, 124310 (2006).

[11] M. G. Silly, J. Roy, H. Enriquez, P. Soukiassian, C. Crotti, S. Fontana, and P. Perfetti, J. Vac. Sci. Technol. B **22**, 2226 (2004); V. Derycke, P. Soukiassian, A. Mayne, G. Dujardin, and J. Gautier, Phys. Rev. Lett. **81**, 5868 (1998).

[12] F. Varchon, P. Mallet, L. Magaud, and J. Y. Veuillen, Phys. Rev. B **77**, 165415 (2008).

[13] D. A. Siegel, S. Y. Zhou, F. El Gabaly, A. K. Schmid, K. F. McCarty, and A. Lanzara, Phys. Rev. B **80**, 241407(R) (2009).

[14] H. Hibino, H. Kageshima, F. Maeda, M. Nagase, Y. Kobayashi, and H. Yamaguchi, Phys. Rev. B **77**, 075413 (2008).

[15] C. Coletti, C. L. Frewin, S. E. Saddow, M. Hetzel, C. Virojanadara, and U. Starke, Appl. Phys. Lett. **91**, 061914 (2007).

[16] J. Penuelas, A. Ouerghi, D. Lucot, C. David, J. Gierack, H. Estrade-Szwarckopf, and C. Andreazza-Vignolle, Phys. Rev. B **79**, 033408 (2009).

[17] T. Seyller, K. V. Emtsev, K. Gao, F. Speck, L. Ley, A. Tadish, L. Broekman, J. D. Riley, R. C. G. Leckey, O. Rader, A. Varykhalov, and A. M. Shikin, Surf. Sci. **600**, 3906 (2006).

[18] Z. H. Ni, W. Chen, X. F. Fan, J. L. Kuo, T. Yu, A. T. S. Wee, and Z. X. Shen, Phys. Rev. B **77**, 115416 (2008); A. C. Ferrari and J. Robertson, *ibid.* **61**, 14095 (2000).

[19] J. Röhl, M. Hundhausen, K. V. Emstev, Th. Seyller, R. Graupner, and L. Ley, Appl. Phys. Lett. **92**, 201918 (2008).

[20] N. Ferralis, R. Maboudian, and C. Carraro, Phys. Rev. Lett. **101**, 156801 (2008).

[21] K. V. Emtsev, F. Speck, Th. Seyller, L. Ley, and J. D. Riley, Phys. Rev. B **77**, 155303 (2008).

[22] U. Starke and C Riedl, J. Phys.: Condens. Matter **21**, 134016 (2009).

[23] F. Varchon, R. Feng, J. Hass, X. Li, B. N. Nguyen, C. Naud, P. Mallet, J.-Y. Veuillen, C. Berger, E. H. Conrad, and L. Magaud, Phys. Rev. Lett. **99**, 126805 (2007).

[24] J. Hass, R. Feng, T. Li, Z. Zong, W. A. de Heer, P. N. First, E. H. Conrad, C. A. Jeffrey, and C. Berger, Appl. Phys. Lett. **89**, 143106 (2006).

[25] M. Suemitsu and H. Fukidome, J. Phys. D **43**, 374012 (2010).

[26] A. Ouerghi, M. Marangolo, R. Belkhou, S. El Moussaoui, M. G. Silly, M. Eddrief, L. Largeau, M. Portail, B. Fain, and F. Sirotti, Phys. Rev. B **82**, 125445 (2010).

[27] A. Michon, S. Vézian, A. Ouerghi, M. Zielinski, T. Chassagne, and M. Portail, Appl. Phys. Lett. **97**, 171909 (2010).

[28] I. Deretzis and A. La Magna, Appl. Phys. Lett. **95**, 063111 (2009).

[29] F. Hiebel, P. Mallet, F. Varchon, L. Magaud, and J. Y. Veuillen, Phys. Rev. B **78**, 153412 (2008).